POLITECNICO
MILANO 1863

SCUOLA DI INGEGNERIA INDUSTRIALE
E DELL'INFORMAZIONE

Executive Summary of the Thesis

A Novel Sector-Based Radiomic Approach to Assess Atherosclerotic Carotid Plaque Dynamics

Laurea Magistrale in Biomedical Engineering - Information Bioengineering

Author: Marina De Santis

Advisor: Prof. Valentina Corino

Co-advisor: Prof. Anna Corti

Academic year: 2025-2026

1. Introduction

Atherosclerosis is a leading cause of death and long-term disability worldwide, and an estimated 10-20% of ischaemic strokes are attributable to carotid artery disease. Early detection of vulnerable plaque, defined as rupture-prone lesions, is therefore crucial for the prevention of major cerebrovascular events. Traditionally, disease severity and treatment decisions have relied on the degree of luminal stenosis; however, it is now recognized that stenosis alone is insufficient for accurate patient risk stratification. With the advent and widespread use of computed tomography angiography (CTA), there is growing interest in identifying reliable non-invasive imaging biomarkers of plaque vulnerability. Histopathological studies have shown that culprit plaques share recurring features, including the presence of a lipid-rich necrotic core, a thin fibrous cap, intraplaque haemorrhage, and calcifications. Notably, while larger calcifications have been associated with plaque stabilization, micro- or spotty calcifications, particularly those close to the lumen, have been linked to increased vulnerability [1].

In this context, radiomics offers a novel opportunity to quantitively capture these characteristics and to describe the mechanism driving morphological and compositional changes of the carotid plaque over time, moving beyond stenosis-based classification. Consistent with the shift, Vacca et al. in a recent systematic review summarized radiomic studies based on CTA scans, as used in this work. So far, most of these studies have focused on distinguishing symptomatic from asymptomatic patients, and only Le et al. have developed a model to identify culprit from non-culprit arteries [3].

The objective of this thesis is to investigate how baseline radiomic features extracted from CTA relate to the longitudinal morphological evolution of carotid plaques. To this end, a novel sector-based radiomic approach was proposed, and three biomarkers of plaque vulnerability were analysed: calcification thickness (CT) variation, lumen-to-calcification distance (CD) variation, and plaque wall thickness (WT) variation. These outcomes were first characterised through exploratory statistical association and subsequently used as targets in machine learning models to derive radiomic signatures of plaque progression or regression. Furthermore, the potential role of radiomics in identifying culprit from non-culprit side in symptomatic patients

was assessed.
In parallel, and using the same patient cohort, Tzioutziou et al. investigated the impact of pressure- and flow-driven biomechanical factors on carotid plaque evolution [2]. The present work complements that biomechanical perspective by focusing on CTA-based radiomic biomarkers, ultimately aiming to integrate radiomics and biomechanical factors into a more comprehensive understanding of plaque vulnerability.

2. Materials and Methods

2.1. Patient dataset

The present study included 75 patients from the Plaque At RISK (PARISK) study, a prospective multicenter (4 hospitals) cohort study of symptomatic patients not scheduled for carotid endarterectomy or stenting. Due to missing imaging or segmentations, 14 patients were excluded, yielding a final sample of 61 patients. All patients had experienced a recent ($<$ 3 months) large artery ischaemic event before the baseline multi-detector CTA (MDCTA) and presented a ipsilateral mild-to-moderate carotid stenosis ($<$ 70%) at enrolment. Both baseline and follow-up bilateral MDCTA were acquired, yielding a final dataset of 122 carotid arteries. All participants provided written informed consent; the study procedures were conducted in accordance with the ethical principles of the Declaration of Helsinki and were approved by the Institutional Review Board.

2.2. Sectorization of the artery

Carotid arteries were semi-automatically segmented from MDCTA images using QAngioCT (Medis, version 3.2.0.13). Lumen, vessel wall, and calcifications were identified bilaterally at baseline and follow-up using standard Hounsfield Unit thresholds, and visually verified by an expert observer. For each patient, baseline and follow-up 3D geometries were co-registered and aligned using the reconstructed lumen centerline and an iterative closest point algorithm implemented in an in-house Python pipeline.
To characterise spatial heterogeneity and enable local radiomic, morphological, and compositional analysis, the carotid artery was sectorised using the Vascular Modelling Toolkit (VMTK, http://www.vmtk.org/). The external carotid artery was excluded, and the lumen centerline served as reference for partitioning. Along the longitudinal axis, the vessel was divided into 1-mm segments, and each cross-section was further subdivided into eight 45° sectors, yielding elementary sectors of 1 mm $\times$ 45° (*Figure 1*). The vessel wall between luminal and outer contours within each sector defined the volumetric regions of interest (ROIs) for radiomic extraction. The entire sectorization process was fully automated within a custom Python pipeline.

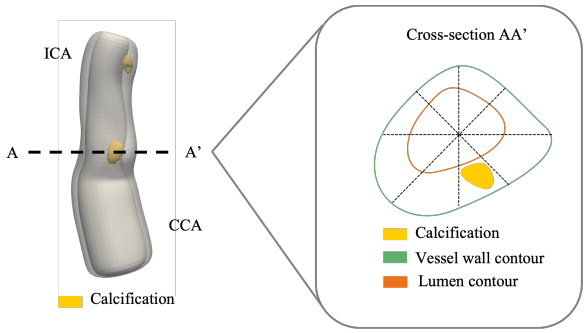

Figure 1: 3D reconstruction of the carotid artery with illustration of the sector-based analysis.

2.3. Radiomic analysis

Radiomic analysis was performed on each sector of the carotid artery wall. Three steps of image preprocessing were applied to MDCTA images, to reduce all the image-related source of variability: (i) 3D Gaussian filter with a 3×3×3 voxel kernel ($\sigma = 0.5$); (ii) fixed-bin histogram discretization, with a bin width of 25; (iii) voxel size resampling to [0.25, 0.25, 0.5] mm using B-spline interpolation. The radiomic analysis was performed using the open-source software PyRadiomics (version 2.2.0). A total of 93 radiomic features were computed from the original MDCTA image, including 18 first order statistics, and 75 textural features.

2.4. Morphometric outcomes

Morphometrics of the carotid artery were computed for each sector at both baseline and follow-up. A ray-casting strategy was implemented: for each point of the lumen, a ray was casted outwards and the intersections with the outer-wall surface and with the calcification were recorded. Therefore, plaque wall thickness was defined

as the radial distance between the lumen surface and the outer-wall surface, while lumen-to-calcification distance as the radial distance between the lumen surface and the calcification. For calcium thickness instead, the radial distance between the lumen surface and the inner boundary of calcification, as well as between the lumen surface and the outer boundary of the same calcification, were measured. Thus, the absolute calcium thickness was obtained by subtracting the inner distance from the outer one (*Figure 2*). Longitudinal changes in plaque wall thickness (ΔWT), lumen-to-calcification distance (ΔCD), and calcium thickness (ΔCT) were assessed by subtracting the baseline values from those at 2-year follow-up. The computation was based on the method described by Tziotziou et al. and was fully automated through an in-house developed Python script.

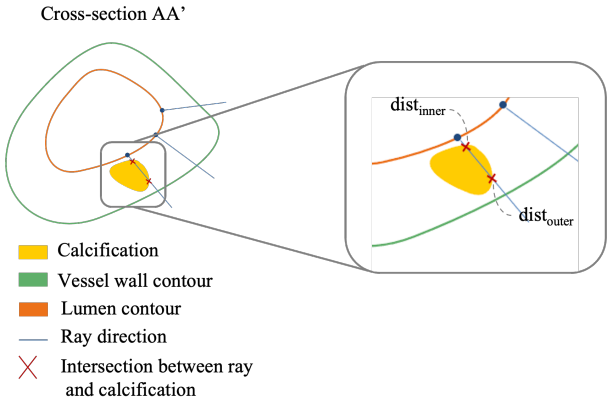

Figure 2: 3D reconstruction of the carotid artery with illustration of the sector-based analysis.

2.5. Statistical analysis

Statistical analyses were performed in Python. Radiomic features were standardised (robust scaling) and pre-screened using pairwise Pearson correlation ($|r| > 0.9$), retaining within each correlated pair the feature less correlated with the remaining set. Vessel sectors were classified as plaque-free or plaque-containing based on local wall thickness, with values > 1.5 mm considered as plaque, and both morphometric and radiomic features were stratified into tertiles, consistent with Tziotziou et al. The predictive value of radiomic features for morphometric evolution was assessed using odds ratios (ORs), while differences across tertiles were tested with the Kruskal-Wallis test. Statistical significance was set at $p < 0.05$ after correction for multiple comparisons.

2.6. Machine learning model development

Separate machine learning models were trained for each of the outcomes. The workflow consisted of three main steps: (i) data splitting, (ii) feature selection, and (iii) model training and evaluation, including within-centre and cross-centre experiments.

First, the dataset was randomly split into a training set (80%) and a held-out test set (20%). All choices regarding feature selection and model configuration were performed exclusively on the training set to avoid information leakage. A 5-fold cross-validation (CV) scheme was adopted on the training set: in each fold, four folds were used for model fitting and one fold for validation. Feature selection was embedded within the CV procedure. Four selection strategies were evaluated: random forest (RF), Least Absolute Shrinkage and Selection Operator (LASSO), minimum redundancy maximum relevance (mRMR), and recursive feature elimination with a support vector machine (RFE-SVM). For each strategy and each CV fold, a subset of informative features was identified, and the optimal subset was constructed with features selected in at least 3 out of the 5 CV folds.

For each selector, several classifiers were then trained: RF, logistic regression (LR), SVM, eXtreme Gradient Boosting (XGBoost), and a soft-voting ensemble combining RF, SVM, and XGBoost. All models were implemented with class weights to mitigate the impact of class imbalance. Performance in each CV fold was quantified using balanced accuracy, and the best selector-classifier combination was identified based on the average balanced accuracy across folds. This optimal configuration was subsequently retrained on the entire training set to exploit all available data, and then evaluated on the independent test set.

Given the multicentric design of the study, additional training-testing schemes were implemented to assess generalizability across centers. Models were trained on different combinations of centers (e.g., single-center or multi-center training) and tested on a distinct external center. Both within-center and cross-center perfor-

mances were reported, and confidence intervals were estimated using bootstrap resampling of the test predictions.

3. Results

Out of the sectorization process, 30927 sectors were generated. Among these, 24% ($n = 7310$) were classified as plaque-containing and constituted the subset used for all downstream analyses. After the decorrelation step, 58 out of the 93 extracted features were retained and used for both exploratory and predictive modeling.

3.1. Calcification thickness variation

Calcified sectors showed a median calcification thickness change of 0.02 mm (IQR: $[-0.12, 0.33]$), with 56% of them exhibiting progression. Exploratory analysis indicated that the features most strongly associated with ΔCT tertiles were textural, in particular *ngtdm_Complexity*, *glszm_GrayLevelNonUniformityNormalized*, and *glcm_DifferenceEntropy*.
Tables 1 and 2 report the performance of the models trained on single-center and multi-center data on the internal and external test sets, respectively.

	AUC	BA	F1
single	0.86	0.81	0.84
	[0.83–0.89]	[0.79–0.84]	[0.83–0.87]
multi	0.80	0.76	0.76
	[0.74–0.85]	[0.70–0.81]	[0.72–0.83]

Table 1: Internal test performance of single- and multi-center trained models.

	AUC	BA	F1
single	0.81	0.74	0.69
	[0.80–0.83]	[0.72–0.75]	[0.68–0.72]
multi	0.83	0.77	0.75
	[0.81–0.84]	[0.75–0.78]	[0.73–0.77]

Table 2: External test performance of single- and multi-center trained models.

3.2. Lumen-to-calcification distance variation

Calcified plaque sectors showed a median lumen-calcium distance change of −0.02 mm (IQR: $[-0.12, 0.13]$), with 54% of them exhibiting a reduction in distance. Exploratory analysis indicated that the features most strongly associated with ΔCD tertiles were *ngtdm_Complexity*, *glszm_GrayLevelNonUniformityNormalized*, and *glcm_ClusterProminence*.
Tables 3 and 4 report the performance of models trained on single-center and multi-center data on the internal and external test sets, respectively.

	AUC	BA	F1
single	0.90	0.86	0.90
	[0.89–0.93]	[0.85–0.88]	[0.88–0.92]
multi	0.87	0.79	0.81
	[0.84–0.92]	[0.76–0.85]	[0.80–0.86]

Table 3: Internal test performance of single- and multi-center trained models.

	AUC	BA	F1
single	0.84	0.78	0.74
	[0.82–0.85]	[0.77–0.79]	[0.73–0.75]
multi	0.85	0.79	0.79
	[0.84–0.86]	[0.78–0.80]	[0.76–0.80]

Table 4: External test performance of single- and multi-center trained models.

3.3. Plaque wall thickness variation

Plaque-containing sectors showed a median wall thickness change of 0.03 mm (IQR: $[-0.29, 0.30]$), with 48% of them exhibiting a reduction. Exploratory analysis indicated that the features most strongly associated with ΔWT tertiles were textural, in particular *gldm_SmallDependenceLowGrayLevelEmphasis*, *glcm_Idmn*, and *glcm_Correlation*.
Tables 5 and 6 report the performance of the models trained on single-center and multi-center data on the internal and external test sets, respectively.

	AUC	BA	F1
single	0.62	0.55	0.64
	[0.60–0.65]	[0.53–0.58]	[0.58–0.70]
multi	0.64	0.58	0.54
	[0.58–0.65]	[0.54–0.62]	[0.50–0.57]

Table 5: Internal test performance of single- and multi-center trained models.

	AUC	BA	F1
single	0.56	0.54	0.53
	[0.53–0.59]	[0.53–0.57]	[0.49–0.57]
multi	0.56	0.57	0.57
	[0.52–0.60]	[0.53–0.59]	[0.53–0.61]

Table 6: External test performance of single- and multi-center trained models.

3.4. Culprit carotid artery classification

Radiomic and integrated models were trained to discriminate culprit from non-culprit carotid arteries in symptomatic patients. The integrated model combined radiomics with baseline morphometrics (CT, CD, WT).
Tables 7 and 8 report the performance of the best radiomic-only and integrated models on the internal and external test sets, respectively.

	AUC	BA	F1
radiomic	0.69	0.73	0.73
	[0.51–0.85]	[0.57–0.87]	[0.60–0.87]
integrated	0.84	0.82	0.82
	[0.70–0.94]	[0.71–0.89]	[0.69–0.89]

Table 7: Internal test performance of radiomic and integrated models.

	AUC	BA	F1
radiomic	0.53	0.57	0.57
	[0.39–0.70]	[0.43–0.71]	[0.45–0.71]
integrated	0.65	0.71	0.72
	[0.52–0.79]	[0.57–0.75]	[0.58–0.80]

Table 8: External test performance of radiomic and integrated models.

4. Discussion

In the present thesis, a novel sector-based radiomic approach was proposed to investigate the local association between baseline radiomic features and carotid morphological changes over 2-year follow-up. The method relied on dividing each carotid artery into unit sectors of 1 mm $\times$ 45°, enabling the characterization of local remodeling patterns associated with atherosclerosis mechanism. The selection of the investigated morphometrics was motivated by current evidence that stenosis alone is insufficient for patient risk stratification, whereas additional biomarkers reflecting plaque vulnerability, have proven meaningful. Accordingly, three morphometrics outcomes were analysed: calcification thickness change, lumen-to-calcification distance change and plaque wall thickness change.
The exploratory analysis revealed that several radiomic features, primarily texture-based features, were strongly associated with local morphometric changes. Associations were particularly pronounced for calcification-related outcomes, where effect sizes were higher and the most significant features largely overleaped between ΔCT and ΔCD, likely reflecting shared information derived from the underlying calcified structure. Conversely, associations with ΔWT were modest, indicating that these changes are less well captured by radiomics alone.
For the predictive modeling task, morphometric variables were dichotomized to distinguish sectors exhibiting an increase from those exhibiting a decrease, with the aim of capturing the directionality of plaque remodeling. Initially, models were trained using data from a single center and evaluated both internally and on external datasets. Internal performance was high for ΔCT and ΔCD, while, consistent with the exploratory findings, ΔWT proved more challenging to predict. However, when tested on external centers, all single-center models experienced a drop in performance, likely reflecting heterogeneity in patient population, scanner vendors, imaging protocols, and acquisitions settings.
To address this limitation, models were subsequently trained on combined multi-center dataset to increase heterogeneity and improve generalization. For ΔCT, multi-center training yielded a modest improvement in cross-center performance, with F1-score increasing from 0.69 to 0.75. Similarly, predictive performance for ΔCD improved from 0.74 to 0.79. In contrast, for ΔWT metrics remained low regardless of training configuration (0.53 vs 0.57), highlighting the inherit difficulty of modeling this outcome. Overall, the multicenter design proved beneficial: the availability of an external held-out center enabled robust evaluation, and training on heterogeneous datasets consistently improved generalisability across centers.
For culprit carotid artery classification, the

radiomic-only model showed modest discrimination. Building on current knowledge of plaque vulnerability, radiomic features were combined with vulnerability-related variables in the integrated model, namely CT, CD and WT variable at baseline. The integrated model achieved strong performance on the internal test set (AUC = 0.84, F1 = 0.80), while external performance decreased to 0.72. Evaluation across different center combinations revealed that some centers were intrinsically more challenging to predict, and incorporating them into training set did not translate into better generalization, suggesting center-specific variability.

To the best of author's knowledge, this work introduces two major novelties. First, it proposes a novel methodology of local radiomic features, differing from conventional plaque radiomic studies which consider features extracted from the entire plaque volume. Second, it focuses on longitudinal evolution of plaque morphology, particularly calcification dynamics whose role in plaque homeostasis and vulnerability remains debated. Previous studies have applied radiomics to classify symptomatic versus asymptomatic patients or to distinguish culprit from non-culprit plaques. In particular, the study by Le at al. reported an AUC of 0.73, comparable to the 0.72 achieved externally in this study; however the integrated model presented here reached an AUC of 0.83 on the internal test set [3].

This study has several limitations. First, patient sample was relatively small ($n = 61$). However, the subdivision of each artery enlarged the dataset to 7310 sectors, ensuring a robust analysis. Second, textural features struggled to characterise wall thickness change, and additional features derived from filters or wavelet transformations were not computed due to computational burden at the sector level. Furthermore, the models did not incorporate clinical covariates, stenosis degree, or additional vulnerability characteristics, and a direct comparison with conventional radiomic on the entire plaque was also not explored. Finally, morphometric computation depends on the reconstructed 3D geometries, and dichotomisation of continuos variables may have reduced information content.

Future work should focus on expanding the dataset, extracting additional radiomic features and modeling continuos morphometric outcomes to preserve information. Moreover, the parallel biomechanical study by Tziotziou et al., although methodologically different, converges with the present work by analysing carotid plaque remodeling through pressure- and flow-driven biomechanical factors. A natural forward step would be to integrate radiomics and biomechanical markers into a comprehensive longitudinal investigation of carotid plaque remodeling.

5. Conclusions

In conclusion, this study explored the association between MDCTA-derived radiomic features and longitudinal changes in plaque morphometrics, supporting their potential role as non-invasive imaging biomarkers. The findings provide insight into the role of radiomics in carotid plaque progression and culprit-side identification, and contribute to the broader effort of moving beyond stenosis in risk stratification. Nevertheless, to move closer to clinical translation, radiomic models will need to be integrated with clinical covariates and biomechanical factors, thereby strengthening the robustness and interpretability of predictions in real-world patient management.

References

[1] L. Saba, T. Saam, H. R. Jäger, C. Yuan, T. S. Hatsukami, D. Saloner, B. A. Wasserman, L. H. Bonati, and M. Wintermark. Imaging biomarkers of vulnerable carotid plaques for stroke risk prediction and their potential clinical implications, 2019.

[2] A. Tziotziou, Y. Liu, F. Fontana, J. Bierens, P. J. Nederkoorn, P. A. de Jong, M. E. Kooi, W. Mess, A. van der Lugt, A. F. W. van der Steen, D. Bos, J. J. Wentzel, and A. C. Akyildiz. Pressure- and flow-driven biomechanical factors associate with carotid atherosclerosis assessed by computed tomography angiography, 2025.

[3] S. Vacca, R. Scicolone, A. Gupta, B. Allan Wasserman, J. Song, V. Nardi, Q. Yang, J. Benson, G. Lanzino, K. Paraskevas, J. S. Suri, and L. Saba. Atherosclerotic carotid artery disease Radiomics: A systematic review with meta-analysis and radiomic quality score assessment, 2024.